



Effect of Polyaniline on Magnetic and Microwave Absorption Properties in $\text{SrFe}_{12}\text{O}_{19}/\text{Zn}_{0.4}\text{Co}_{0.2}\text{Ni}_{0.4}\text{Fe}_2\text{O}_4$ Ferrite Nanocomposites

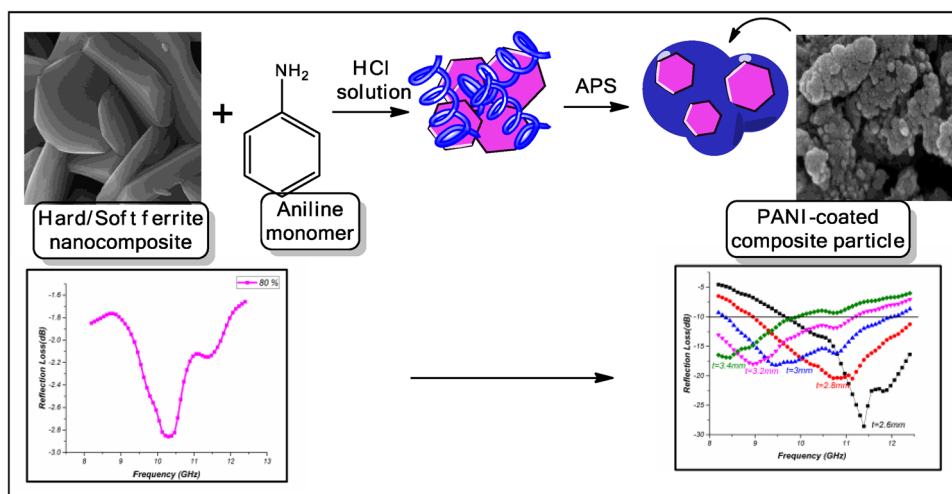
Faezeh Tavakolinia¹ · Mohammad Yousefi² · Seyyed Salman Seyyed Afghahi³ · Saeid Baghshahi⁴ · Susan Samadi²

Received: 9 February 2020 / Accepted: 12 April 2020 / Published online: 8 May 2020
© Springer Science+Business Media, LLC, part of Springer Nature 2020

Abstract

Polyaniline PANI/ $(\text{SrFe}_{12}\text{O}_{19})_{(1-x)}/(\text{Co}_{0.8}\text{Ni}_{0.2}\text{Fe}_2\text{O}_4)_x$ ($x = 0.2, 0.4, 0.6, 0.8$) composites were prepared via the in situ polymerization process. The structure, morphology and electromagnetic absorption properties of samples were studied. XRD (x-ray diffractometer), FESEM (field emission scanning electron microscopy), and FTIR (field transform infrared) analyses demonstrated that $\text{SrFe}_{12}\text{O}_{19}/\text{Zn}_{0.4}\text{Co}_{0.2}\text{Ni}_{0.4}\text{Fe}_2\text{O}_4$ ferrite particles were covered by PANI coating. VSM measurement revealed by adding non-magnetic polymer (PANI), magnetic features of aimed composites declined. The electromagnetic absorption of synthesized samples was measured by VNA. In the frequency range of 8.2–12.4 GHz (X-Band), the reflection loss improved to -28.5 dB from -2.93 dB composites of PANI/ $(\text{SrFe}_{12}\text{O}_{19})_{0.2}/(\text{Zn}_{0.4}\text{Co}_{0.2}\text{Ni}_{0.4}\text{Fe}_2\text{O}_4)_{0.8}$ in comparison to $(\text{SrFe}_{12}\text{O}_{19})_{0.2}/(\text{Zn}_{0.4}\text{Co}_{0.2}\text{Ni}_{0.4}\text{Fe}_2\text{O}_4)_{0.8}$. Due to the perfect impedance matching between PANI as the dielectric part, and ferrites in the case of the magnetic part, the reflection loss decreased in PANI/ $(\text{SrFe}_{12}\text{O}_{19})_{(1-x)}/(\text{Co}_{0.8}\text{Ni}_{0.2}\text{Fe}_2\text{O}_4)_x$ composites. The minimum reflection loss of the PANI/ $\text{SrFe}_{12}\text{O}_{19}/\text{Zn}_{0.4}\text{Co}_{0.2}\text{Ni}_{0.4}\text{Fe}_2\text{O}_4$ composites was -28.6 dB at the frequency of 11.5 GHz.

Graphic Abstract



Keywords Hard/soft composites · Magnetisation · Polyaniline · Reflection loss · Impedance matching

1 Introduction

Microwave-absorbing materials have been developed recently for military stealth applications and the hindrance of electromagnetic interferences. Conducting polymer

✉ Mohammad Yousefi
myousefi50@hotmail.com

Extended author information available on the last page of the article

nanocomposites such as polyaniline and polythiophene have been utilized in remarkable domains as microwave absorbing materials, batteries, and shielding equipment [1, 2]. Polyaniline with high electrical conductivity, easy preparation, and excellent environmental stability is one of the promising candidates for microwave absorption applications [3, 4]. The magnetic fillers such as soft spinel ferrite and hard M-type ferrite with high saturation magnetization, stability, and high remanence were added to the polymer for enhancing the electromagnetic absorption properties [5–7].

Various methods like polymerization, microemulsion polymerization, electrochemical, and electrospinning, were used for preparing polymer/ferrite nanocomposites [8–11]. Among them, the sol–gel process was a cost-effective and affordable preparation of ferrites that fabricated prominent microwave-absorbing material with special properties as lessened thickness, wider bandwidth, and adjustable impedance matching properties (matching dielectric and magnetic part). A combination of conducting polymer with hard ($\text{SrFe}_{12}\text{O}_{19}$) and soft ferrite ($\text{Zn}_{0.4}\text{Co}_{0.2}\text{Ni}_{0.4}\text{Fe}_2\text{O}_4$) improved reaching these properties. Hard and soft ferrites with a high dielectric part should have been compatible with perfect impedance matching [12–15]. In spite of diverse investigations on magnetic absorbers, there was the requirement for synthesizing materials that possessed the highest absorbing properties, which will absorb in an intended frequency.

In this article, the nanocomposites of hard ($\text{SrFe}_{12}\text{O}_{19}$)/soft ferrite ($\text{Zn}_{0.4}\text{Co}_{0.2}\text{Ni}_{0.4}\text{Fe}_2\text{O}_4$) have been prepared by the sol–gel process, and then PANI/ $(\text{SrFe}_{12}\text{O}_{19})_{(1-x)}/(\text{Zn}_{0.4}\text{Co}_{0.2}\text{Ni}_{0.4}\text{Fe}_2\text{O}_4)_x$ ($x = 0.2, 0.4, 0.6, 0.8$) was produced by the in situ polymerization method. These samples are unique and represent excellent electrical conductivity and electromagnetic properties, which significantly increased the complex permittivity of the composite and provided the material with interesting shielding properties. The structure and morphology were characterized by various experimental techniques, and the properties of the composite were investigated.

2 Experimental

2.1 Materials

Twice-distilled aniline monomer, ammonium peroxydisulfate ($(\text{NH}_4)_2\text{S}_2\text{O}_8$, APS), iron nitrate ninehydrate ($\text{Fe}(\text{NO}_3)_3 \cdot 9\text{H}_2\text{O}$), strontium nitrate ($\text{Sr}(\text{NO}_3)_2$), zinc chloride (ZnCl_2), cobalt nitrate hexahydrate ($\text{Co}(\text{NO}_3)_2 \cdot 6\text{H}_2\text{O}$), nickel nitrate hexahydrate ($\text{Ni}(\text{NO}_3)_2 \cdot 6\text{H}_2\text{O}$) and citric acid ($\text{C}_6\text{H}_8\text{O}_7 \cdot \text{H}_2\text{O}$) (Merck) were utilized without further purification.

2.2 Preparation of PANI/ $(\text{SrFe}_{12}\text{O}_{19})_{(1-x)}/(\text{Zn}_{0.4}\text{Co}_{0.2}\text{Ni}_{0.4}\text{Fe}_2\text{O}_4)_x$ ($x = 0.2, 0.4, 0.6, 0.8$)

PANI/ $(\text{SrFe}_{12}\text{O}_{19})_{(1-x)}/(\text{Zn}_{0.4}\text{Co}_{0.2}\text{Ni}_{0.4}\text{Fe}_2\text{O}_4)_x$ ferrite composites were prepared by in situ polymerization. A stoichiometric amount of $(\text{SrFe}_{12}\text{O}_{19})_{(1-x)}/(\text{Zn}_{0.4}\text{Co}_{0.2}\text{Ni}_{0.4}\text{Fe}_2\text{O}_4)_x$ ferrite particles and aniline monomer were exposed to ultrasound for 30 min. $(\text{SrFe}_{12}\text{O}_{19})_{(1-x)}/(\text{Zn}_{0.4}\text{Co}_{0.2}\text{Ni}_{0.4}\text{Fe}_2\text{O}_4)_x$ ferrite particles were prepared through the authors' previous literature that labels of samples (80%, 60%, 40% and 20% soft) were shown in Table 1 [16].

4.98 g of APS was dissolved in a 40 mL 0.1 M HCl solution, then added slowly to the ferrites and an aniline solution. The polymerization was accomplished at 0–5 °C for 12 h. The composite was obtained by filtering and washing in three steps, (1 M HCl, distilled water and finally ethanol) for removing all unwanted compounds. The samples dried under vacuum at 60 °C for 24 h. The Schematic representation of PANI coating with $(\text{SrFe}_{12}\text{O}_{19})_{(1-x)}/(\text{Zn}_{0.4}\text{Co}_{0.2}\text{Ni}_{0.4}\text{Fe}_2\text{O}_4)_x$ ($x = 0.2, 0.4, 0.6, 0.8$) composites was illustrated in Fig. 1. The specimen's codes of samples coated by PANI are obvious in Table 1.

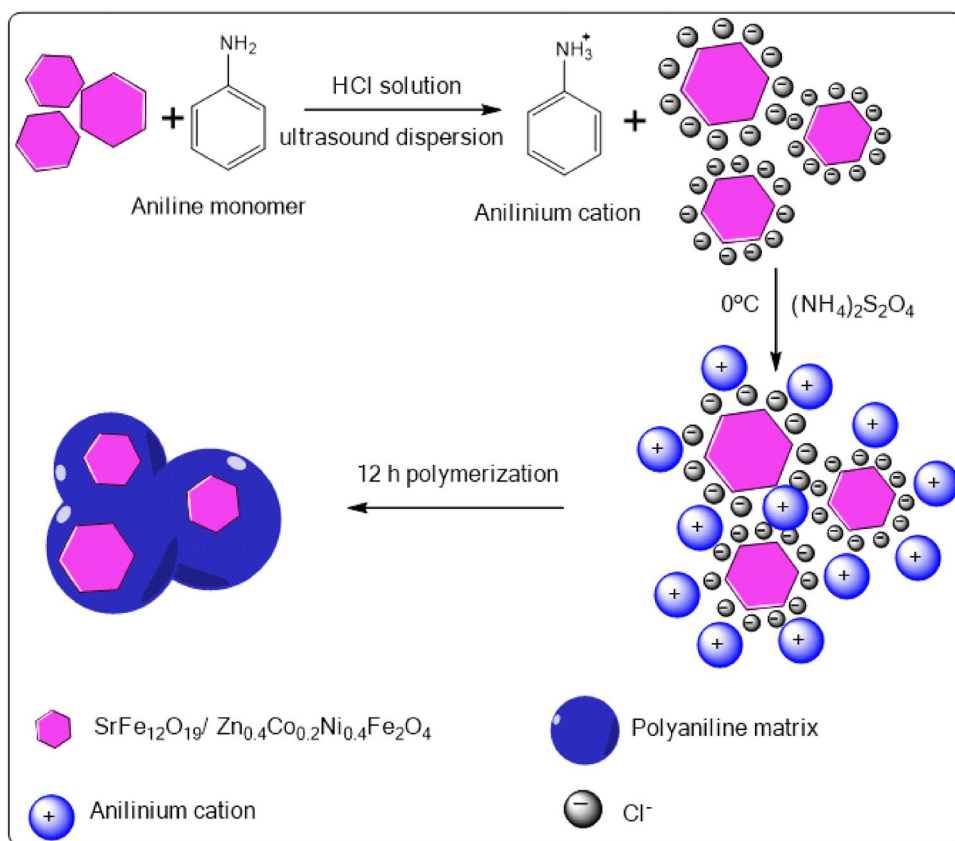
2.3 Characterization

X-ray diffraction (XRD) (Model: XPERT-MPD, Philips) with Cu K α radiation ($\lambda = 1.5418 \text{ \AA}$) over the 2θ range of 10–80° with a step size of 0.5 was used in order to investigate phase hexaferrites structure. A field emission scanning electron microscope (FESEM, SIGMA, VP-500, ZEISS model) was employed for investigating the morphology of products. The magnetic properties of samples were characterized by a Lake Shore 7307 vibrating sample magnetometer (VSM). Microwave absorption, permittivity ($\epsilon = \epsilon' - i\epsilon''$) and permeability ($\mu = \mu' - i\mu''$) in the range of X bands frequency were measured with a vector network analyzer (VNA, Agilent 8510C). The preparation of synthesized compounds for electromagnetic absorption measurements was performed by

Table 1 Specimen's codes of samples

Sample	Sample code
PANI/ $(\text{Zn}_{0.4}\text{Co}_{0.2}\text{Ni}_{0.4}\text{Fe}_2\text{O}_4)_{0.8}(\text{SrFe}_{12}\text{O}_{19})_{0.2}$	80% + PANI
PANI/ $(\text{Zn}_{0.4}\text{Co}_{0.2}\text{Ni}_{0.4}\text{Fe}_2\text{O}_4)_{0.6}(\text{SrFe}_{12}\text{O}_{19})_{0.4}$	60% + PANI
PANI/ $(\text{Zn}_{0.4}\text{Co}_{0.2}\text{Ni}_{0.4}\text{Fe}_2\text{O}_4)_{0.4}(\text{SrFe}_{12}\text{O}_{19})_{0.6}$	40% + PANI
PANI/ $(\text{Zn}_{0.4}\text{Co}_{0.2}\text{Ni}_{0.4}\text{Fe}_2\text{O}_4)_{0.2}(\text{SrFe}_{12}\text{O}_{19})_{0.8}$	20% + PANI
$(\text{Zn}_{0.4}\text{Co}_{0.2}\text{Ni}_{0.4}\text{Fe}_2\text{O}_4)_{0.8}(\text{SrFe}_{12}\text{O}_{19})_{0.2}$	80% soft
$(\text{Zn}_{0.4}\text{Co}_{0.2}\text{Ni}_{0.4}\text{Fe}_2\text{O}_4)_{0.6}(\text{SrFe}_{12}\text{O}_{19})_{0.4}$	60% soft
$(\text{Zn}_{0.4}\text{Co}_{0.2}\text{Ni}_{0.4}\text{Fe}_2\text{O}_4)_{0.4}(\text{SrFe}_{12}\text{O}_{19})_{0.6}$	40% soft
$(\text{Zn}_{0.4}\text{Co}_{0.2}\text{Ni}_{0.4}\text{Fe}_2\text{O}_4)_{0.2}(\text{SrFe}_{12}\text{O}_{19})_{0.8}$	20% soft

Fig. 1 Schematic representation of PANI coating with $(\text{SrFe}_{12}\text{O}_{19})_{(1-x)}/(\text{Zn}_{0.4}\text{Co}_{0.2}\text{Ni}_{0.4}\text{Fe}_2\text{O}_4)_{(x)}$ composites



mixing composites with paraffin (mass ratio, composite/Paraffin:70/30). The samples were molded in the rectangular template with $22.86 \times 10.16 \times 1 \text{ mm}^3$ diameter.

3 Results and Discussion

3.1 XRD Analysis

The XRD pattern of PANI- $\text{SrFe}_{12}\text{O}_{19}/\text{Zn}_{0.4}\text{Co}_{0.2}\text{Ni}_{0.4}\text{Fe}_2\text{O}_4$ ferrite (Fig. 2a) and $\text{SrFe}_{12}\text{O}_{19}/\text{Zn}_{0.4}\text{Co}_{0.2}\text{Ni}_{0.4}\text{Fe}_2\text{O}_4$ ferrite (Fig. 2b) versus soft-phase content in the composite was shown in Fig. 2. It is known that the structure of PANI is principally amorphous. The broad peaks at about $2\theta = 20.6^\circ, 25.4^\circ$ are related to the amorphous properties of PANI polymer. Due to the effect of PANI on the crystallization of $\text{SrFe}_{12}\text{O}_{19}/\text{Zn}_{0.4}\text{Co}_{0.2}\text{Ni}_{0.4}\text{Fe}_2\text{O}_4$, the intensities of PANI composites peaks rise more than $\text{SrFe}_{12}\text{O}_{19}/\text{Zn}_{0.4}\text{Co}_{0.2}\text{Ni}_{0.4}\text{Fe}_2\text{O}_4$ composites [17].

As shown in Fig. 2b, all peaks of the $\text{SrFe}_{12}\text{O}_{19}/\text{Zn}_{0.4}\text{Co}_{0.2}\text{Ni}_{0.4}\text{Fe}_2\text{O}_4$ ferrite can be seen, which accord well with the standard JCPDS card No. 01–084–1531 for $\text{SrFe}_{12}\text{O}_{19}$ and $\text{Zn}_{0.4}\text{Co}_{0.2}\text{Ni}_{0.4}\text{Fe}_2\text{O}_4$ (JCPDS card No. 01–087–2336) [18]. The broad peaks (shown in Fig. 2b) at

about $2\theta = 20.6^\circ, 25.4^\circ$ show amorphous nature ascribed to the parallel and perpendicular periodicity of the PANI chains. The diffraction peaks for nanocomposite in Fig. 2a–d exhibits the characteristic peaks of PANI/ $(\text{SrFe}_{12}\text{O}_{19})_{(1-x)}/(\text{Co}_{0.8}\text{Ni}_{0.2}\text{Fe}_2\text{O}_4)_{(x)}$ ferrite. In addition, the intensities of all the peaks for the composite are higher than those of the pure ferrites, which reveal that the PANI coating layer has an effect on the crystallinity of $(\text{SrFe}_{12}\text{O}_{19})_{(1-x)}/(\text{Co}_{0.8}\text{Ni}_{0.2}\text{Fe}_2\text{O}_4)_{(x)}$ ferrite. All these reveal the formation of the PANI/ $(\text{SrFe}_{12}\text{O}_{19})_{(1-x)}/(\text{Co}_{0.8}\text{Ni}_{0.2}\text{Fe}_2\text{O}_4)_{(x)}$ ferrite nanocomposite is complete [19, 20].

3.2 IR Spectra

Figure 3 demonstrates the IR spectra of PANI/ $(\text{SrFe}_{12}\text{O}_{19})_{(1-x)}/(\text{Zn}_{0.4}\text{Co}_{0.2}\text{Ni}_{0.4}\text{Fe}_2\text{O}_4)_{(x)}$ ferrites versus soft phase content in the composite. In Fig. 3 (20% + PANI, 40% + PANI, 60% + PANI, and 80% + PANI), the peaks at 1565 and 1488 cm^{-1} are attributed to stretching vibration of $\text{C}=\text{N}$ and $\text{C}=\text{C}$, the peaks at 1298 and 1234 cm^{-1} are assigned to stretching vibration of the benzenoid rings and quinoid. Moreover, the peaks at 780 cm^{-1} are attributed to the out-of-plane deformation of C-H in the p-disubstituted benzene ring. The spectrum of PANI indicates the

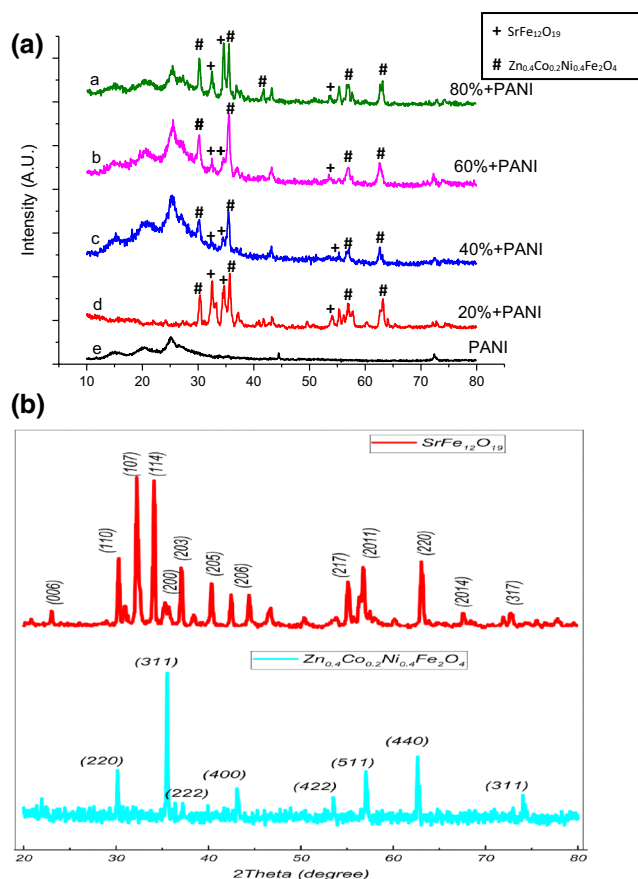


Fig. 2 a XRD patterns of PANI/ $(\text{SrFe}_{12}\text{O}_{19})_{(1-x)}/(\text{Zn}_{0.4}\text{Co}_{0.2}\text{Ni}_{0.4}\text{Fe}_2\text{O}_4)_x$, b XRD patterns of pure $\text{SrFe}_{12}\text{O}_{19}$ and pure $\text{Zn}_{0.4}\text{Co}_{0.2}\text{Ni}_{0.4}\text{Fe}_2\text{O}_4$

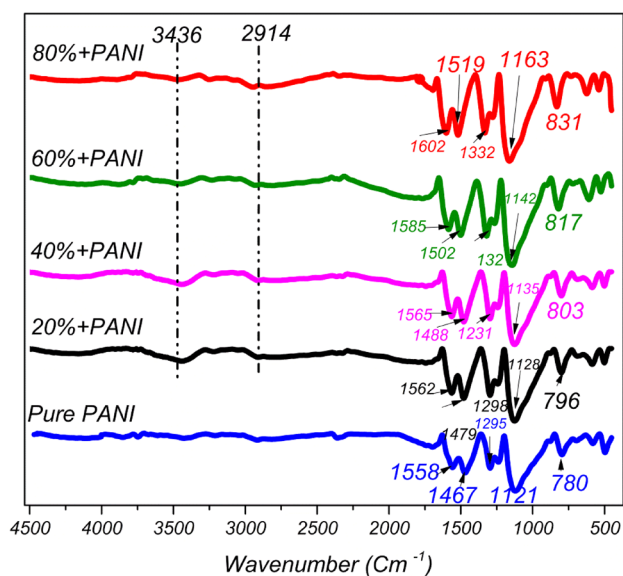


Fig. 3 FTIR Spectra of PANI/ $(\text{SrFe}_{12}\text{O}_{19})_{(1-x)}/(\text{Zn}_{0.4}\text{Co}_{0.2}\text{Ni}_{0.4}\text{Fe}_2\text{O}_4)_x$ composites

characteristic peak located at 3434 cm^{-1} is the stretching vibration of the N–H group. The IR spectrum of PANI- $(\text{SrFe}_{12}\text{O}_{19})_{(1-x)}/(\text{Zn}_{0.4}\text{Co}_{0.2}\text{Ni}_{0.4}\text{Fe}_2\text{O}_4)_x$ ferrite in Fig. 3 is similar to pure PANI, and the characteristic peaks of $(\text{SrFe}_{12}\text{O}_{19})_{(1-x)}/(\text{Zn}_{0.4}\text{Co}_{0.2}\text{Ni}_{0.4}\text{Fe}_2\text{O}_4)_x$ ferrite at 430 cm^{-1} and 588 cm^{-1} can be found, which are attributed to stretching vibration between metal ions and oxygen [21]. The IR Spectra of $(\text{SrFe}_{12}\text{O}_{19})_{(1-x)}/(\text{Zn}_{0.4}\text{Co}_{0.2}\text{Ni}_{0.4}\text{Fe}_2\text{O}_4)_x$ ferrite was reported in our latest work [16]. Compared the FT-IR spectrum of PANI with 20%, 40%, 60% and 80% + PANI (Fig. 3), the peaks at 1558, 1467, 1295, 1121 and 780 cm^{-1} (for pure PANI) are shifted to 1562, 1602, 1470–1519, 1298–1332, 1125–1163 and $796\text{--}831\text{ cm}^{-1}$ in the 20%, 40%, 60% and 80% + PANI composite respectively. In other words, with the increase of the soft phase, the peaks have shifted to higher wave number which emphasise the successful coating of PANI on the surfaces of 20%, 40%, 60% and 80% + PANI composite. The blue shifted of the vibrations indicating that there exists a charge transfer between PANI and $(\text{SrFe}_{12}\text{O}_{19})_{(1-x)}/(\text{Zn}_{0.4}\text{Co}_{0.2}\text{Ni}_{0.4}\text{Fe}_2\text{O}_4)_x$ [22, 23].

3.3 Morphology

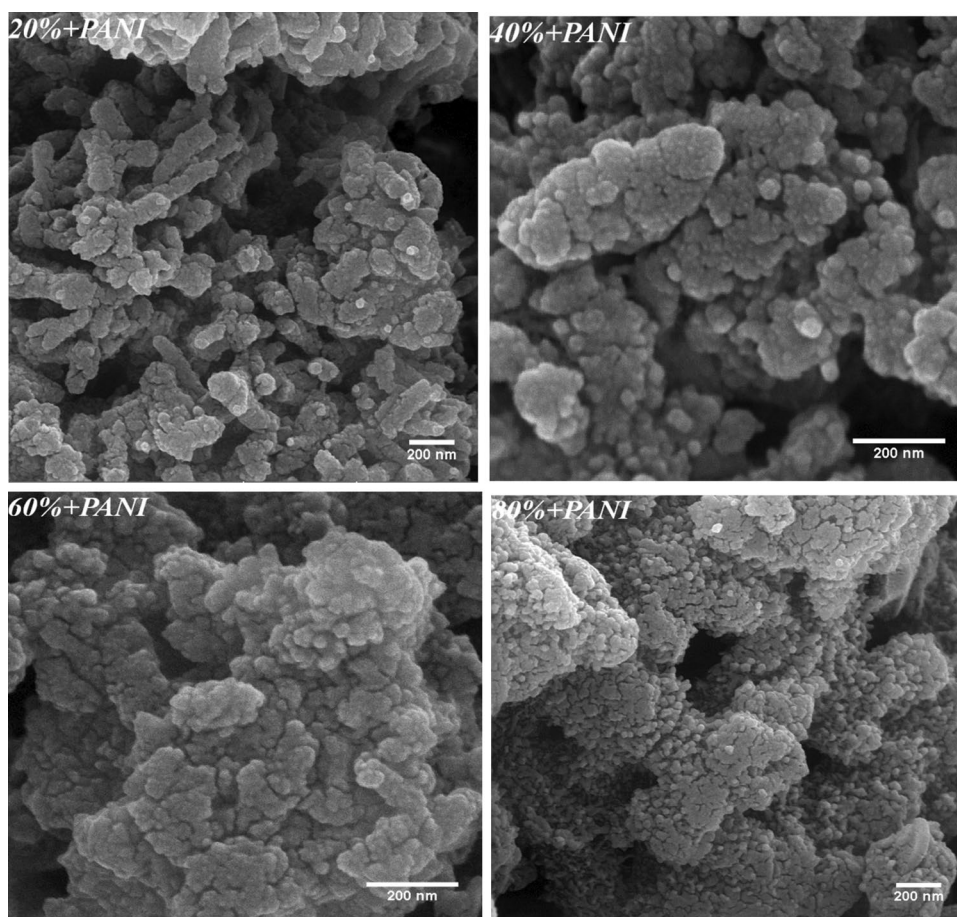
FESEM used to evaluate the surface morphology of the composites powder and PANI in Fig. 4. The FESEM micrographs represented the two phases of ferrite composite and ferrite composite/PANI are well-distributed [24]. The granular grains with small size are of cubic $\text{Zn}_{0.4}\text{Co}_{0.2}\text{Ni}_{0.4}\text{Fe}_2\text{O}_4$ phase while the plate-like grains with a larger size are of hexagonal $\text{SrFe}_{12}\text{O}_{19}$ phase. After coating with PANI, a continuous overlayer of conducting polymers is produced on the surface of $(\text{SrFe}_{12}\text{O}_{19})_{(1-x)}/\text{Zn}_{0.4}\text{Co}_{0.2}\text{Ni}_{0.4}\text{Fe}_2\text{O}_4)_x$ grains. In Fig. 4 uniform PANI nanoparticles are observed which are fully coated on the surface of the composite. $(\text{SrFe}_{12}\text{O}_{19})_{(1-x)}/(\text{Zn}_{0.4}\text{Co}_{0.2}\text{Ni}_{0.4}\text{Fe}_2\text{O}_4)_x$ is apparently not observed, demonstrating that PANI and $(\text{SrFe}_{12}\text{O}_{19})_{(1-x)}/(\text{Zn}_{0.4}\text{Co}_{0.2}\text{Ni}_{0.4}\text{Fe}_2\text{O}_4)_x$ are perfectly assembled.

FESEM micrographs of PANI composites reveal the granular morphology with an average particle size of 316 nm. The rougher surface of PANI/ $(\text{SrFe}_{12}\text{O}_{19})_{(1-x)}/(\text{Zn}_{0.4}\text{Co}_{0.2}\text{Ni}_{0.4}\text{Fe}_2\text{O}_4)_x$ in comparison to $(\text{SrFe}_{12}\text{O}_{19})_{(1-x)}/(\text{Zn}_{0.4}\text{Co}_{0.2}\text{Ni}_{0.4}\text{Fe}_2\text{O}_4)_x$ declared that PANI covered the surface of $(\text{SrFe}_{12}\text{O}_{19})_{(1-x)}/(\text{Zn}_{0.4}\text{Co}_{0.2}\text{Ni}_{0.4}\text{Fe}_2\text{O}_4)_x$ [25].

3.4 Magnetic Properties

The hysteresis loops of PANI/ $(\text{SrFe}_{12}\text{O}_{19})_{(1-x)}/(\text{Zn}_{0.4}\text{Co}_{0.2}\text{Ni}_{0.4}\text{Fe}_2\text{O}_4)_x$ ferrite are shown in Fig. 5. Regarding the addition of non-magnetic PANI to the hard/soft phase, the saturation magnetization (M_s) declined from

Fig. 4 FESEM micrograph of hard-soft ferrite/PANI nanocomposites with different weight ratios of soft ferrite



around 60 in $(\text{SrFe}_{12}\text{O}_{19})_{(1-x)}/(\text{Zn}_{0.4}\text{Co}_{0.2}\text{Ni}_{0.4}\text{Fe}_2\text{O}_4)_x$ ferrite to about 20 emu/g in $\text{PANI}/(\text{SrFe}_{12}\text{O}_{19})_{(1-x)}/(\text{Zn}_{0.4}\text{Co}_{0.2}\text{Ni}_{0.4}\text{Fe}_2\text{O}_4)_x$. Based on the $M_s = \varphi \cdot m_s$ equation [26], in which M_s is related to the volume fraction of the particles (φ) and the saturation moment of a single particle (m_s), reducing the magnetic fraction of ferrite resulted in the decreasing of saturation magnetization. The non-magnetic PANI was found to separate the magnetic grains, which lead to an increase of diamagnetic strength effects, and declined the magnetic properties.

The PANI non-magnetic particles in the composites, it produces a bigger segregation to magnetic grain. All these lead to a stronger demagnetic effect, the magnetic effect of the composites is weaker. The coercive force of the composites has not any significant change. The coercive is related to many factors such as microscopic structure, grain shape, components, magnetic anisotropy (magnetic crystal, stress, shape) and magnetic scalability, etc. In the polymerization process, PANI is deposited on the ferrite surface and crystallite boundary, which will reduce the magnetic surface

anisotropy of ferrite particles. On the other hand, the charge transfer can exist on ferrite surface between ferrite and PANI, which changes the charge density of ferrite surface and affects the electronic spin mechanism of system. All these weaken the domain wall movement of ferrite particles. These two factors have led to nano composites coercive force reduction [27].

For the $\text{PANI}/(\text{SrFe}_{12}\text{O}_{19})_{(1-x)}/(\text{Zn}_{0.4}\text{Co}_{0.2}\text{Ni}_{0.4}\text{Fe}_2\text{O}_4)_x$ composites, firstly, in the polymerization process, PANI is deposited on the $(\text{SrFe}_{12}\text{O}_{19})_{(1-x)}/(\text{Zn}_{0.4}\text{Co}_{0.2}\text{Ni}_{0.4}\text{Fe}_2\text{O}_4)_x$ surface and crystallite boundaries, which would result in an interface effect between the PANI and $(\text{SrFe}_{12}\text{O}_{19})_{(1-x)}/(\text{Zn}_{0.4}\text{Co}_{0.2}\text{Ni}_{0.4}\text{Fe}_2\text{O}_4)_x$, therefore the surface anisotropy of the $\text{PANI}/(\text{SrFe}_{12}\text{O}_{19})_{(1-x)}/(\text{Zn}_{0.4}\text{Co}_{0.2}\text{Ni}_{0.4}\text{Fe}_2\text{O}_4)_x$ composites declines [26]. Secondly, in M-type strontium ferrites, lowering the anisotropy field results in lower natural resonance frequency [28–30]. The PANI coating on the $(\text{SrFe}_{12}\text{O}_{19})_{(1-x)}/(\text{Zn}_{0.4}\text{Co}_{0.2}\text{Ni}_{0.4}\text{Fe}_2\text{O}_4)_x$ composites will likely affect the contributions of the surface anisotropy, shape anisotropy, and interface anisotropy to the net anisotropy [31]. Consequently, the PANI/

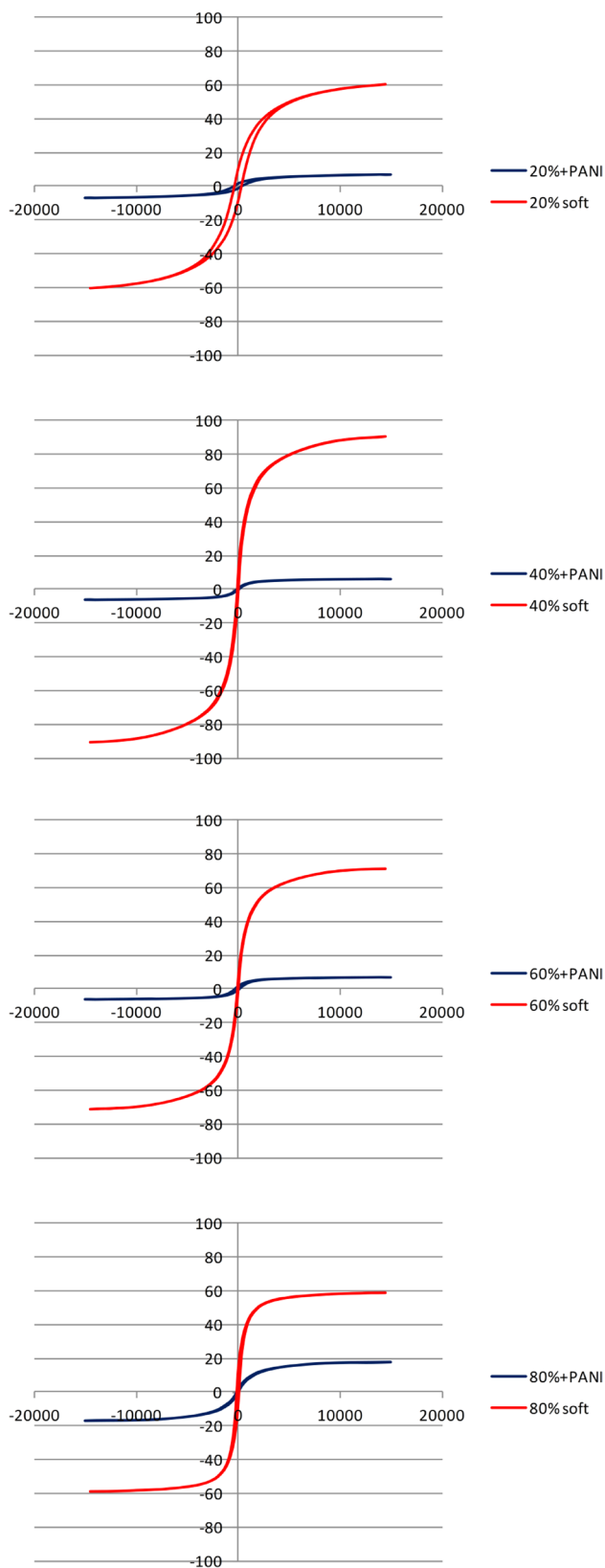


Fig. 5 Magnetic hysteresis loops of hard-soft ferrite [16] and hard-soft ferrite/PANI nanocomposites with different weight ratios of soft ferrite

$(\text{SrFe}_{12}\text{O}_{19})_{(1-x)}/(\text{Zn}_{0.4}\text{Co}_{0.2}\text{Ni}_{0.4}\text{Fe}_2\text{O}_4)_{(x)}$ composites show lower coercivity value compared to that of $(\text{SrFe}_{12}\text{O}_{19})_{(1-x)}/(\text{Zn}_{0.4}\text{Co}_{0.2}\text{Ni}_{0.4}\text{Fe}_2\text{O}_4)_{(x)}$ composites.

Coating the PANI on the ferrite particles reduced the magnetic anisotropy. In the case of PANI composites, the charge-transfer between ferrite and PANI had an influence on the electronic spin mechanism. As a result, the domain wall movement of magnetic particles decreased. Thus, the composites' coercivity was forced to fall [27].

3.5 Electromagnetic Properties Analysis

The electromagnetic parameters of samples between 8.2 GHz and 12.4 GHz are shown in Fig. 6. Obviously, the values of real and imaginary parts of permittivity of composites which were coated by PANI, were higher than $(\text{SrFe}_{12}\text{O}_{19})_{(1-x)}/(\text{Zn}_{0.4}\text{Co}_{0.2}\text{Ni}_{0.4}\text{Fe}_2\text{O}_4)_{(x)}$ samples. The ϵ' values were increased by the coating of PANI, which probably occurred due to the capacitive interaction between non-percolating PANI chains. Also, $(\text{SrFe}_{12}\text{O}_{19})_{(1-x)}/(\text{Zn}_{0.4}\text{Co}_{0.2}\text{Ni}_{0.4}\text{Fe}_2\text{O}_4)_{(x)}$ samples showed comparable ϵ' values in comparison to PANI coated samples, indicating that the interfacial polarization that took place between insulating ferrite particles was important in storing the incident electric field. The imaginary part of permittivity (which represents the dissipation of electromagnetic radiation) was almost zero in all $(\text{SrFe}_{12}\text{O}_{19})_{(1-x)}/(\text{Zn}_{0.4}\text{Co}_{0.2}\text{Ni}_{0.4}\text{Fe}_2\text{O}_4)_{(x)}$ samples, indicating no active electric field dissipation mechanism existed in these specimens. While ϵ' and ϵ'' for PANI coated samples a vast increase was observed, where for 20%, 40% and 80% soft ferrites, the ϵ' and ϵ'' were varied between 2 and 3, and for 60% soft ferrite sample it varied between 3.5–4.5. This could have been attributed to the increase in conductivity of the samples by incorporation of PANI. In fact, the imaginary permittivity (ϵ'') itself is related to electrical conductivity (σ) by the following equation: $\epsilon'' = \sigma/2\pi f\epsilon_0$ [32] which serves to indicate a direct relationship between the two parameters leading to the conductance loss which is expressed as: $\tan(\delta_c) = 1.8 \times 10^{10}\sigma/f\epsilon_r$ [33]. But as will soon be explained, there were no active electrical current based loss mechanisms. The main source for higher dielectric loss in PANI coated samples was, therefore, dielectric relaxation. As depicted by the Cole–Cole equation, the dielectric relaxation in polymers is given by [34].

$$\left[\epsilon' - \frac{\epsilon_s + \epsilon_\infty}{2} \right]^2 + \left[\epsilon'' + \frac{\epsilon_s - \epsilon_\infty}{2} \tan\left(\frac{\pi\alpha}{2}\right) \right]^2 = \left[\frac{\epsilon_s - \epsilon_\infty}{2} \times \frac{1}{\cos(\pi\alpha/2)} \right]^2 \quad (1)$$

where $\omega = 2\pi f$, f is the frequency, ϵ_s and ϵ_∞ are stationary and infinite frequency dielectric constants, τ is the Debye's

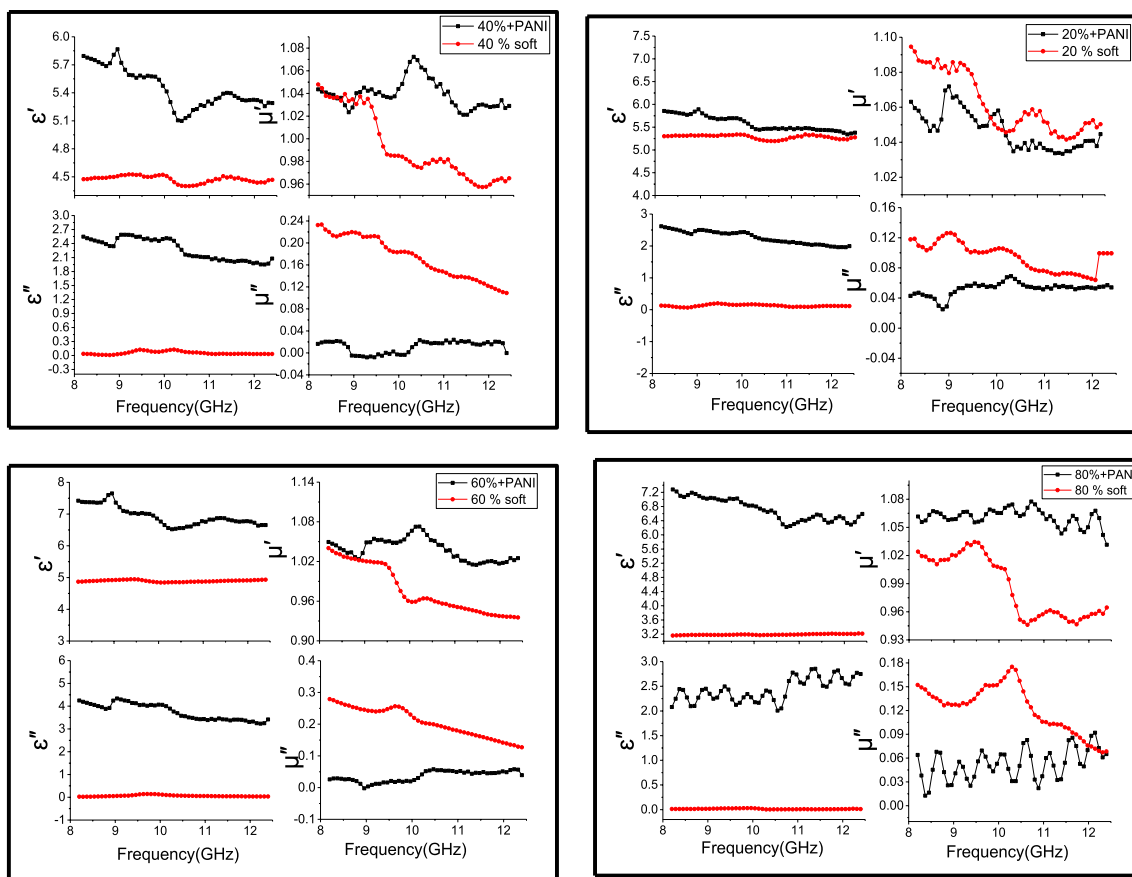


Fig. 6 The relative complex permittivity and permeability of hard-soft ferrite/PANI nanocomposites with different weight ratios of soft ferrite

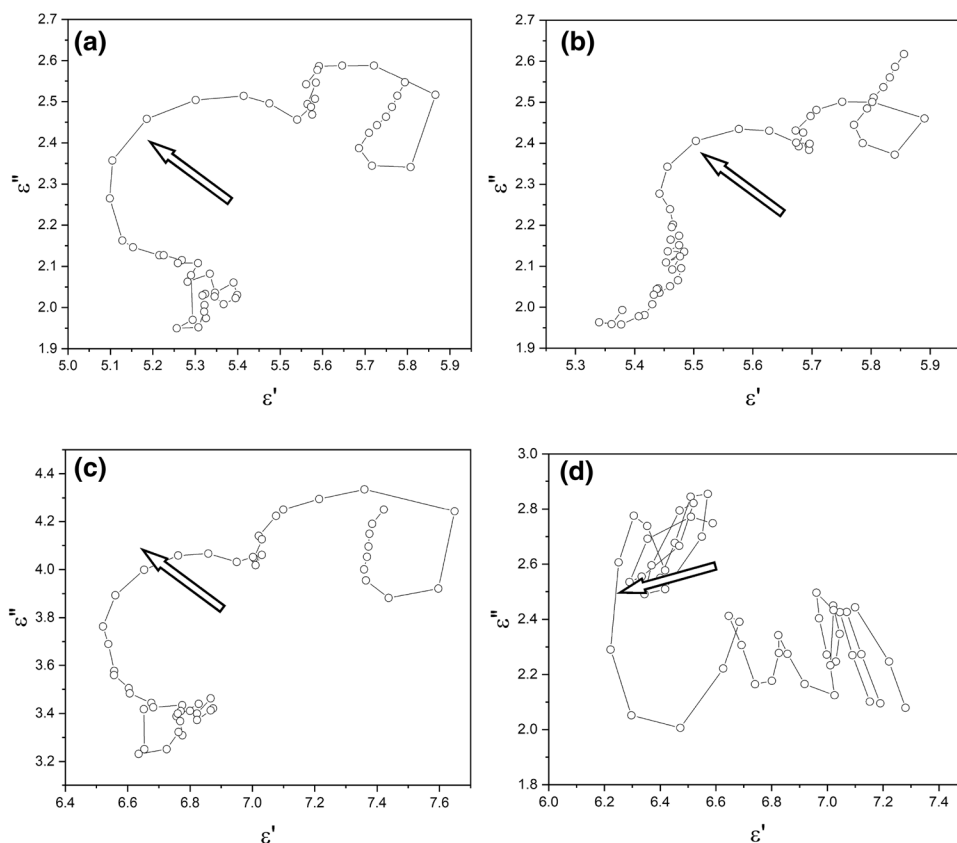
relaxation time and $0 < \alpha < 1$ is the dispersion degree of the Debye's relaxation time as a result of molecular state and interactions, medium type and thermal fluctuations. Therefore, the ϵ'' versus ϵ' is an arc rather than a semicircle which the center of the arc may be out of the plot area. Considering the Cole–Cole plots for PANI coated samples from Fig. 7, it was evident that all PANI coated sample features showed at least one semicircle arc that represented a Debye's dipolar relaxation mechanism.

The dielectric loss tangents of the samples are shown in Fig. 8a. Clearly, the dielectric loss tangent has increased from about 0.03 as a maximum value for non-PANI samples to about 0.65 in 60% + PANI sample which confirms the extensive effect of PANI in enhancing the dielectric loss properties compared to $(\text{SrFe}_{12}\text{O}_{19})_{(1-x)}/(\text{Zn}_{0.4}\text{Co}_{0.2}\text{Ni}_{0.4}\text{Fe}_2\text{O}_4)_{(x)}$ samples, in which the dielectric loss raised only from the $\text{Fe}^{+3}\text{-Fe}^{2+}$ content of ferrite. The

polarization is expected to occur as a result of $\text{Fe}^{+3}\text{-Fe}^{+2}$ charge transfer which causes a local displacement of electrons in the electrical field direction [35].

All samples showed slight variation (between 0.95 and 1.1) of the magnetic field storage capability (μ') in the whole monitored frequency band (Fig. 6), because frequency of the applied field was very high compared to relaxation frequency of magnetic dipoles in $(\text{SrFe}_{12}\text{O}_{19})_{(1-x)}/(\text{Zn}_{0.4}\text{Co}_{0.2}\text{Ni}_{0.4}\text{Fe}_2\text{O}_4)_{(x)}$ ferrite, which indicated almost no storage of the applied oscillating magnetic field. But the loss part of permeability (μ'') was shown to be very higher in $(\text{SrFe}_{12}\text{O}_{19})_{(1-x)}/(\text{Zn}_{0.4}\text{Co}_{0.2}\text{Ni}_{0.4}\text{Fe}_2\text{O}_4)_{(x)}$ samples than PANI coated samples; Since at high frequencies (e.g. GHz range), the main magnetic loss mechanisms are eddy current loss, magnetic resonance and hysteresis loss [36]. $(\text{SrFe}_{12}\text{O}_{19})_{(1-x)}/(\text{Zn}_{0.4}\text{Co}_{0.2}\text{Ni}_{0.4}\text{Fe}_2\text{O}_4)_{(x)}$ samples are insulators, therefore the induction of eddy currents is not possible.

Fig. 7 Cole–Cole plots for PANI coated samples **a** 20% + PANI, **b** 40% + PANI, **c** 60% + PANI, **d** 80% + PANI



There was no resonant absorption peaks for 20% and 40% soft samples (Fig. 8b) and the main absorption mechanism in $(\text{SrFe}_{12}\text{O}_{19})_{(1-x)}/(\text{Zn}_{0.4}\text{Co}_{0.2}\text{Ni}_{0.4}\text{Fe}_2\text{O}_4)_x$ could have been the hysteresis loss due to magnetic surface anisotropy of the synthesized $(\text{SrFe}_{12}\text{O}_{19})_{(1-x)}/(\text{Zn}_{0.4}\text{Co}_{0.2}\text{Ni}_{0.4}\text{Fe}_2\text{O}_4)_x$ hard/soft nanoparticles [33]. However, by increasing the fraction of the soft magnetic phase, samples of 60% and 80% soft showed two peaks in Fig. 8b which indicated the onset of ferrimagnetic resonance. In PANI coated samples, if eddy currents can be considered as a prevailing loss mechanism, the value of $\mu''\mu'^{-2}f^{-1}$ (in nine seconds) should have been constant at the whole frequency domain of the experiment. However, such a condition was not met for any of the PANI coated samples [1, 2, 37, 38]. Finally, considering Fig. 8b we could conclude that the very low values of $\tan \delta_m$ were in fact a sign of the absence of effective magnetic loss mechanisms in the PANI coated sample.

3.6 Microwave Absorption Simulation

The microwave absorption properties of ferrite/PANI composites were represented by the reflection loss (RL). The RL values were calculated with the complex of μ and ϵ at

given thickness d and frequency f , based on the transmission line theory. Usually, the normalized input impedance of a microwave absorptive layer can be calculated by [37, 38]:

$$Z_{in} = Z_0 \sqrt{\mu/\epsilon} \tanh \left[j \frac{2\pi f d \sqrt{\mu\epsilon}}{c} \right] \quad (2)$$

where Z_0 is the intrinsic impedance of free space, ϵ is the complex relative permittivity and μ is the complex relative permeability of the sample, f is the frequency of the electromagnetic wave, d is the thickness of absorber, and c is the velocity of light in vacuum. Based on the transmission line theory, the RL as a function of the normalized input impedance is [39]:

$$\text{RL} = 20 \log \left| \frac{Z_{in} - Z_0}{Z_{in} + Z_0} \right| \quad (3)$$

Figures 9 and 10 represent the dependence of reflection loss on the frequency and thickness of the absorber layer for each of eight uncoated and coated samples with PANI. It is seen that for the 20% soft sample, the minimum RL of -4.2 dB at the thickness of 1 mm, and the frequency of 11.25 GHz is achieved. By increasing the amount of the

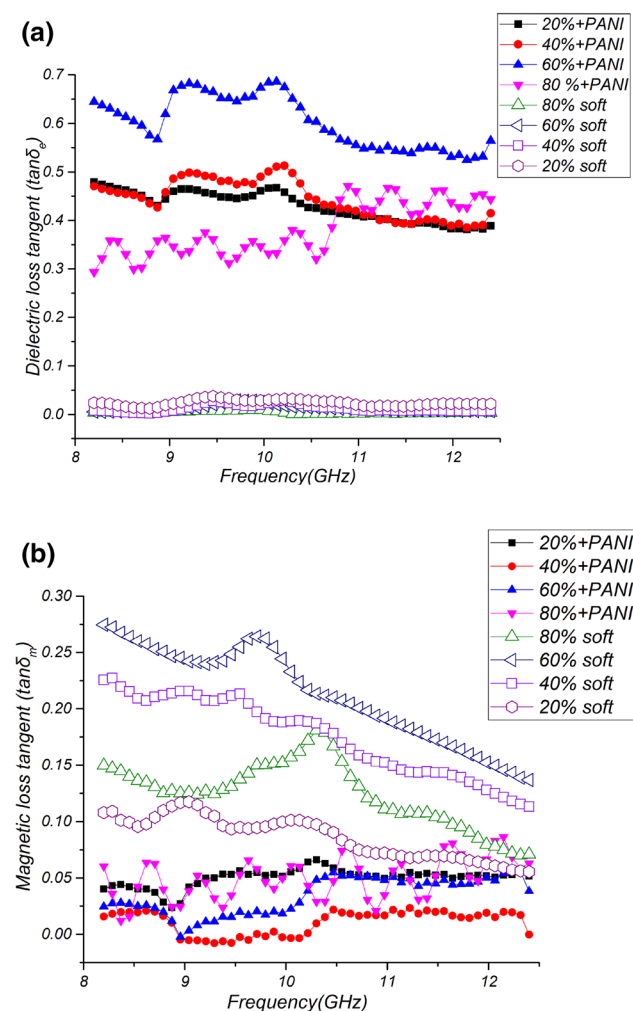


Fig. 8 **a** dielectric and **b** magnetic loss tangents of $(\text{Zn}_{0.4}\text{Co}_{0.2}\text{Ni}_{0.4}\text{Fe}_2\text{O}_4)_x(\text{SrFe}_{12}\text{O}_{19})_{(1-x)}$ and PANI/ $(\text{Zn}_{0.4}\text{Co}_{0.2}\text{Ni}_{0.4}\text{Fe}_2\text{O}_4)_x(\text{SrFe}_{12}\text{O}_{19})_{(1-x)}$ nanocomposites

soft phase from 20 to 40% and 60%, the minimum RL values were increased to -6.8 dB and -9 dB at 1.7 mm and 1.85 mm thicknesses at 11.3 GHz and 11.1 GHz respectively. Greater increase in the amount of the soft phase (to 80%) was found to decrease the minimum RL value to about -4.3 dB at a higher thickness of 2.6 mm at 11.65 GHz.

The first obvious characteristic of uncoated ferrite reflection maps is that the maximum absorption among all these samples was limited to about -9 dB in 60% soft sample, which was mainly due to magnetic loss mechanisms as discussed in the previous section. Also, there was almost zero absorption for the frequencies below 10 GHz for all $(\text{SrFe}_{12}\text{O}_{19})_{(1-x)}/(\text{Zn}_{0.4}\text{Co}_{0.2}\text{Ni}_{0.4}\text{Fe}_2\text{O}_4)_x$ samples and the maximum amount of reflection loss for all $(\text{SrFe}_{12}\text{O}_{19})_{(1-x)}/$

$(\text{Zn}_{0.4}\text{Co}_{0.2}\text{Ni}_{0.4}\text{Fe}_2\text{O}_4)_x$ samples was achieved at thicknesses below 3 mm. This confirms magnetic mechanism as the active dissipation mechanism, since in dielectric absorbers the reflection loss was in direct relationship with the absorber thickness.

In PANI coated samples, the values of reflection loss showed a significant increase as for sample 20% + PANI, a minimum RL of -28 dB was achieved at 2.4 mm thickness at 10.8 GHz. It is noteworthy to mention that for this sample the minimum RL could be maintained below -20 dB at all thicknesses below 2.5 mm and at the higher thicknesses between 2.5 and 5 mm, the minimum reflection loss was below -15 dB. The mean absorption bandwidth (RL < -10 dB) for this sample was about 1 GHz at different thicknesses. The reflection loss pattern for PANI/40% soft sample had many similarities to 20% + PANI, but a weakened version of 20% + PANI sample exhibited a minimum RL of -4 dB at 2.3 mm thickness at 11 GHz. In fact, the RL map showed a little shift to higher frequencies. Also, the mean absorption bandwidth along all thicknesses reduced to below 1 GHz for a 40% + PANI sample. For the 60% + PANI sample, the minimum RL had shifted to higher thicknesses while for 20% and 40% samples the absorption occurred mainly below 2.5 mm for 60% soft and 80% soft samples. We observed the stronger absorption values at thicknesses higher than 3 mm. For both 60% soft and 80% soft samples, the value of minimum RL increased by the thickness and reached its highest value at 5 mm thickness for both samples to -25.5 dB and -38 dB for 60% + PANI and 80% + PANI respectively. Since for all PANI coated samples the minimum RL which could be achieved at each thickness was lower than -20 dB (RL < -20 dB), it could be inferred that the dielectric loss was the governing dissipation mechanism as discussed earlier in Sect. 3.5.

In addition, the mean absorption bandwidth (RL < -10 dB) at different thicknesses was achieved at about 0.9 and 0.8 GHz for 60% soft and 80% soft samples respectively. The minimum RL of -38 dB in 80% + PANI which served as the maximum value amongst all samples was due to the collective effect of high dielectric loss of PANI and higher magnetic loss of 80% soft magnetic phase in contrast to other samples. Since the magnetic dissipation mechanisms were narrowband, it could be assumed that the similar values of absorption bandwidth (between 0.8–1 GHz) in PANI coated samples were attributed to the almost equal amounts of PANI in all PANI coated samples. The summary of achieved data from previous works is revealed in Table 2 which can be compared by this work. This is clear that our prepared composites are more capable as electromagnetic absorber in 2.6 mm.

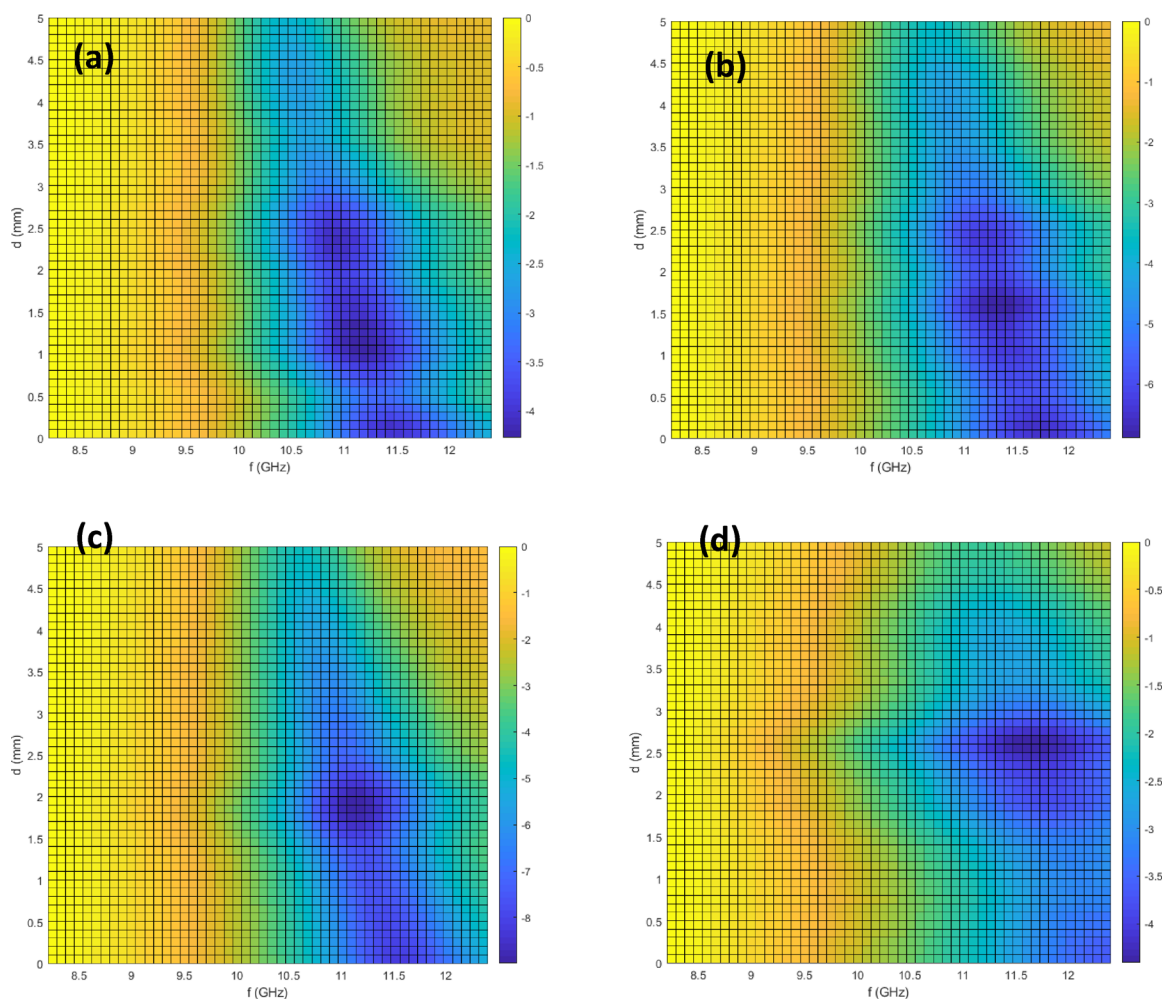


Fig. 9 Simulations for the reflection loss with frequency and thickness of the absorber layer for **a** 20% soft, **b** 40% soft, **c** 60% soft, **d** 80% soft (Continued)

4 Conclusions

PANI/(SrFe₁₂O₁₉)_(1-x)/(Zn_{0.4}Co_{0.2}Ni_{0.4}Fe₂O₄)_(x) composites were prepared successfully by in situ polymerization method. The results of XRD, FTIR, and FESEM revealed the formation of the PANI/(SrFe₁₂O₁₉)_(1-x)/(Zn_{0.4}Co_{0.2}Ni_{0.4}Fe₂O₄)_(x) ferrite composites. The electrical conductivity of the composites was higher than (SrFe₁₂O₁₉)_(1-x)/(Zn_{0.2}Co_{0.8}Ni_{0.2}Fe₂O₄)_(x) and the magnetic properties were in the opposite tendency. A minimum reflection loss of the

PANI/(SrFe₁₂O₁₉)_(1-x)/(Zn_{0.4}Co_{0.2}Ni_{0.4}Fe₂O₄)_(x) composites with 80% soft phase was -28.5 dB at 11.39 GHz at 2.6 mm. By increasing the soft phase at high frequencies, the minimum RL was observed in low thickness and vice versa. The introduction of PANI improved the absorbing properties, which was due to the dielectric loss of PANI. Therefore, it can be concluded that the prepared composites do in fact have potential applications in EMI shielding.

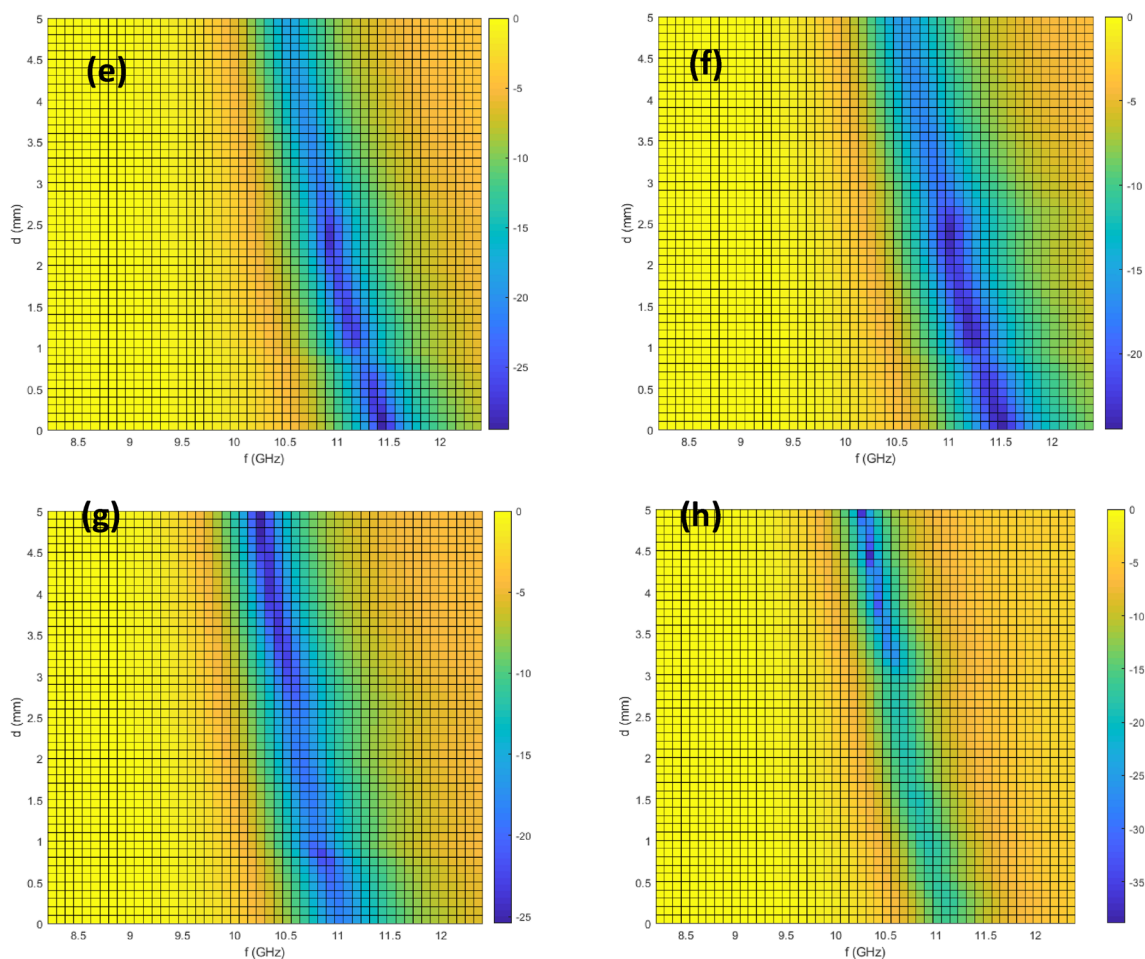


Fig. 10 Simulations for the reflection loss with frequency and thickness of the absorber layer for **e** 20% + PANI, **f** 40% + PANI, **g** 60% + PANI, **h** 80% + PANI

Table 2 Summary of previous works and the comparison of achieved data with our work

Sample	Minimum RL value dB	Minimum RL frequency GHz	Thickness mm	Effective bandwidth (GHz) (RL < -10 dB)	References
BaFe ₁₂ O ₁₉ /Ni _{0.8} Zn _{0.2} Fe ₂ O ₄ /PANI	-22	12.5	2.5	1	[10]
FeNi/PANI	-2.1	11.9	3		[40]
ATP/BaFe ₁₂ O ₁₉ /PANI	-12.5	-7	3	2.5	[41]
BaFe ₁₂ O ₁₉ /PANI	-12	21.5	2	2	[4]
CoFe ₂ O ₄ /EG/PANI	-19.13	13.28	0.5	5.94	[26]
Ni _{0.5} Zn _{0.5} Fe ₂ O ₄ /PANI	-20	9.1	2	0.5	[42]
MnFe ₂ O ₄ /PANI	-15.3	10.4	1.4		[21]
PANI/(SrFe ₁₂ O ₁₉) _{0.2} /(Zn _{0.4} Co _{0.2} Ni _{0.4} Fe ₂ O ₄) _{0.8}	-28.5	11.39	2.6	2.9	This work

References

- D.W. Gu, J.S. Li, J.L. Liu, Y.M. Cai, L.J. Shen, Polyaniline thin films in situ polymerized under very high pressure. *Synth. Met.* **150**, 175–179 (2005). <https://doi.org/10.1016/j.synthmet.2005.02.009>
- Q. Li, C. Zhang, Y. Wang, B. Li, Preparation and characterization of flake-like polypyrrole/SrFe₂O₁₉ composites with different surface active agents. *Synth. Met.* **159**, 2029–2033 (2009). <https://doi.org/10.1016/j.synthmet.2009.07.025>
- J. Jiang, C. Chen, L.H. Ai, L.C. Li, H. Liu, Synthesis and characterization of novel ferromagnetic PPy-based nanocomposite. *Mater. Lett.* **63**, 560–562 (2009). <https://doi.org/10.1016/j.matlet.2008.11.031>
- T. Ting, K. Wu, Synthesis, characterization of polyaniline/BaFe₂O₁₉ composites with microwave-absorbing properties. *J. Magn. Mater.* **322**, 2160–2166 (2010). <https://doi.org/10.1016/j.jmmm.2010.02.002>
- A.H. Abdalsalam, A.A. Ati, A. Abduljabbar, T. Ali, Structural, Optical, Electrical and Magnetic Studies of PANI/Ferrite Nanocomposites Synthesized by PLD Technique. *J. Inorg. Organomet. Polym. Mater.* (2018). <https://doi.org/10.1007/s10904-018-0997-2>
- Y. Sen, S. Xiaoping, D. Youwei, Exchange coupled Nd₂Fe₁₄B/ α -Fe nanocomposite magnets with fine α -Fe grains. *Microelectron. Eng.* **66**, 121–127 (2003). [https://doi.org/10.1016/S0167-9317\(03\)00035-2](https://doi.org/10.1016/S0167-9317(03)00035-2)
- G. Mu, X. Pan, N. Chen, C. He, M. Gu, Synthesis and characterization of hard magnetic composites—Hollow microsphere/titania/barium ferrite. *Appl. Surf. Sci.* **254**, 2483–2486 (2008). <https://doi.org/10.1016/j.apsusc.2007.09.076>
- S. Bose, T. Kuila, M.E. Uddin, N.H. Kim, A.K.T. Lau, J.H. Lee, In-situ synthesis and characterization of electrically conductive polypyrrole/graphene nanocomposites. *Polymer (Guildf)*. **51**, 5921–5928 (2010). <https://doi.org/10.1016/j.polymer.2010.10.014>
- J. Chen, Z. Zhang, Radiation-induced polymerization of methyl methacrylate in microemulsion with high monomer content. *Eur. Polym. J.* **43**, 1188–1194 (2007). <https://doi.org/10.1016/j.eurpolymj.2007.01.049>
- Y. Wang, Y. Huang, Q. Wang, Q. He, L. Chen, Preparation and electromagnetic properties of Polyaniline(polypyrrole)—BaFe₂O₁₉/Ni_{0.8}Zn_{0.2}Fe₂O₄ferrite nanocomposites. *Appl. Surf. Sci.* **259**, 486–493 (2012). <https://doi.org/10.1016/j.apsusc.2012.07.072>
- L. Van Der Schueren, B. De Schoenmaker, Ö.I. Kalaoglu, K. De Clerck, An alternative solvent system for the steady state electrospinning of polycaprolactone. *Eur. Polym. J.* **47**, 1256–1263 (2011). <https://doi.org/10.1016/j.eurpolymj.2011.02.025>
- H. Kavas, A. Baykal, A. Demir, M.S. Toprak, B. Aktas, Zn x Cu (1 2 x) Fe 2 O 4 Nanoferrites by Sol—Gel Auto Combustion Route : Cation Distribution and Microwave Absorption Properties. *J. Inorg. Organomet. Polym. Mater.* (2014). <https://doi.org/10.1007/s10904-014-0069-1>
- A. Baykal, F. Genc, A.Z. Elmal, S. Go, M. Sertkol, H. So, MnCr x Fe 2 2 x O 4 Nanoparticles : Magnetic and microwave absorption properties. *J. Inorg. Organomet. Polym. Mater.* (2015). <https://doi.org/10.1007/s10904-015-0288-0>
- Y. Li, R. Yi, A. Yan, L. Deng, K. Zhou, X. Liu, Facile synthesis and properties of ZnFe₂O₄ and ZnFe₂O₄/polypyrrole core-shell nanoparticles. *Solid State Sci.* **11**, 1319–1324 (2009). <https://doi.org/10.1016/j.solidstatesciences.2009.04.014>
- R. Moučka, M. Mravčáková, J. Vilčáková, M. Omastová, P. Sába, Electromagnetic absorption efficiency of polypropylene/montmorillonite/polypyrrole nanocomposites. *Mater. Des.* **32**, 2006–2011 (2011). <https://doi.org/10.1016/j.matdes.2010.11.064>
- F. Tavakolinia, M. Yousefi, S. Salman, S. Afghahi, S. Baghshahi, S. Samadi, Synthesis of novel hard/soft ferrite composites particles with improved magnetic properties and exchange coupling. *Process. Appl. Ceram.* **12**(3), 248–256 (2018)
- J. Jiang, L. Ai, L. Li, Synthesis and characterization of polyaniline-based nanocomposites containing magnetic Li-Ni-La ferrite. *J. Non. Cryst. Solids.* **355**, 1733–1736 (2009). <https://doi.org/10.1016/j.jnoncrysol.2009.06.012>
- P. Kaur, S.K. Chawla, S.B. Narang, K. Pubby, Structural, magnetic and microwave absorption behavior of Co-Zr substituted strontium hexaferrites prepared using tartaric acid fuel for electromagnetic interference suppression. *J. Magn. Mater.* **422**, 304–314 (2017). <https://doi.org/10.1016/j.jmmm.2016.08.095>
- S. Hazra, B.K. Ghosh, M.K. Patra, R.K. Jani, S.R. Vadera, N.N. Ghosh, A novel ‘one-pot’ synthetic method for preparation of (Ni_{0.65}Zn_{0.35}Fe₂O₄)_x-(BaFe₂O₁₉)_{1-x} nanocomposites and study of their microwave absorption and magnetic properties. *Powder Technol.* **279**, 10–17 (2015). <https://doi.org/10.1016/j.powtec.2015.03.046>
- F. Huixia, B. Dezhong, T. Lin, C. Nali, W. Yueyi, F. Huixia, B. Dezhong, T. Lin, C. Nali, Preparation and microwave-absorbing property of EP/BaFe₂O₁₉/PANI composites. *J. Magn. Mater.* (2016). <https://doi.org/10.1016/j.jmmm.2016.12.118>
- S.H. Hosseini, S.H. Mohseni, A. Asadnia, H. Kerdari, Synthesis and microwave absorbing properties of polyaniline/MnFe₂O₄ nanocomposite. *J. Alloys Compd.* **509**, 4682–4687 (2011). <https://doi.org/10.1016/j.jallcom.2010.11.198>
- Y. Wang, Y. Huang, J. Ding, Synthesis and electromagnetic absorption properties of polypyrrole/BaFe₂O₁₉-Ni_{0.8}Zn_{0.2}Fe₂O₄/multi-walled carbon nanotube composites. *Mater. Sci. Semicond. Process.* **26**, 632–641 (2014). <https://doi.org/10.1016/j.mssp.2014.06.001>
- Z. Li, H. Zhang, Q. Liu, Y. Liu, L. Stanciu, Covalently-grafted polyaniline on graphene oxide sheets for high performance electrochemical supercapacitors. *Carbon N. Y.* **71**, 257–267 (2014). <https://doi.org/10.1016/j.carbon.2014.01.037>
- H. Sozeri, U. Kurtan, R. Topkaya, A. Baykal, M.S. Toprak, Polyaniline (PANI)-Co_{0.5}Mn_{0.5}Fe₂O₄ nanocomposite: Synthesis, characterization and magnetic properties evaluation. *Ceram. Int.* **39**, 5137–5143 (2013). <https://doi.org/10.1016/j.ceramint.2012.12.009>
- L.I. Liangchao, Q.I.U. Haizhen, W. Yuping, Preparation and magnetic properties of Cu_{0.4}Zn_{0.6}Cr_{0.5}Mn_{0.6}Fe_{1.44}O₄/polyaniline nanocomposites. *J. Rare Earths.* **26**, 558–562 (2008)
- Q. XuF, K. Chen, C. Xiang, L. Li, H. Qian, A novel ternary composite: fabrication, performance and application of expanded graphite/polyaniline/CoFe₂O₄ ferrite. *J. Mater. Chem.* **22**(13), 6449–6455 (2012). <https://doi.org/10.1039/c2jm15096d>
- J. Jiang, L. Li, F. Xu, Polyaniline-LiNi ferrite core-shell composite: Preparation, characterization and properties. *Mater. Sci. Eng. A.* **456**, 300–304 (2007). <https://doi.org/10.1016/j.msea.2006.11.143>
- H. Zhu, H. Lin, H. Guo, L. Yu, Microwave absorbing property of Fe-filled carbon nanotubes synthesized by a practical route. *Mat. Sci. Eng. B* **138**, 101–104 (2007). <https://doi.org/10.1016/j.mseb.2006.12.018>
- K. Park, S. Lee, C. Kim, J. Han, Fabrication and electromagnetic characteristics of electromagnetic wave absorbing sandwich structures. *Comp. Sci. Technol.* **66**, 576–584 (2006). <https://doi.org/10.1016/j.compscitech.2005.05.034>
- P. Singh, V.K. Babbar, A. Razdan, R.K. Puri, T.C. Goel, P. Singh, Complex permittivity, permeability, and X-band microwave absorption of CaCoTi ferrite composites Complex permittivity, permeability, and X-band microwave absorption of CaCoTi ferrite composites. *J. App. Phy.* **4362**, 2–7 (2011). <https://doi.org/10.1063/1.373079>

31. P. Xu, X. Han, J. Jiang, X. Wang, X. Li, A. Wen, Synthesis and Characterization of Novel Coraloid Polyaniline/BaFe₁₂O₁₉ Nanocomposites. *J. Phys. Chem. C*. **111**(34), 12603–12608 (2007)
32. L. Olmedo, G. Chateau, C. Deleuze, J.L. Forveille, L. Olmedo, G. Chateau, C. Deleuze, J.L. Forveille, Microwave characterization and modelization of magnetic granular materials. *J. App. Phy.* **6992**, 126–129 (1993). <https://doi.org/10.1063/1.352408>
33. J. Huo, L. Wang, H. Yu, Polymeric nanocomposites for electromagnetic wave absorption. *J. Mater. Sci.* **44**, 3917–3927 (2009). <https://doi.org/10.1007/s10853-009-3561-1>
34. A. Shokuhfar, S.S.S. Afghahi, Two step synthesis, electromagnetic and microwave absorbing properties of FeCo @ C core—shell nanostructure. *J. Magn. Magn. Mater.* (2014). <https://doi.org/10.1016/j.jmmm.2014.06.040>
35. P. Chitra, A. Muthusamy, S. Dineshkumar, Journal of Magnetism and Magnetic Materials Temperature and frequency dependence on electrical properties of polyaniline/Ni (1 Å x) Co x Fe₂O₄ nanocomposites. *J. Magn. Magn. Mater.* **384**, 204–212 (2015). <https://doi.org/10.1016/j.jmmm.2015.02.040>
36. S. Salman, S. Afghahi, R. Peymanfar, S. Javanshir, Y. Atassi, Synthesis, Characterization and Microwave Characteristics of Ternary Nanocomposite of MWCNTs/doped Srhexaferrite/PANI. *J. Magn. Magn. Mater.* (2016). <https://doi.org/10.1016/j.jmmm.2016.09.082>
37. Z. Kessler, Electrical Conductivity in Heterogeneous Polymer Systems V (1): Further Experimental Evidence for a Phase Transition at the Critical Concentration. *Eng. Sci Polym* (1991). <https://doi.org/10.1002/pen.760311608>
38. S.S. Kim, S.B. Jo, K.I. Gueon, K.K. Choi, J.M. Kim, K.S. Churn, Complex permeability and permittivity and microwave absorption of ferrite-rubber composite at X-band frequencies. *IEEE Trans. Magn.* **27**, 5462–5464 (1991). <https://doi.org/10.1109/20.278872>
39. Y. Naito, K. Suetake, Application of ferrite to electromagnetic wave absorber and its characteristics. *IEEE Trans. Microw. Theory Tech.* **19**, 65–72 (1971). <https://doi.org/10.1109/TMTT.1971.1127446>
40. M. Almasi-Kashi, M.H. Mokarian, S. Alikhanzadeh-Arani, Improvement of the microwave absorption properties in FeNi/PANI nanocomposites fabricated with different structures. *J. Alloys Compd.* **742**, 413–420 (2018). <https://doi.org/10.1016/j.jallcom.2018.01.294>
41. D. Bai, H. Feng, N. Chen, L. Tan, J. Qiu, Synthesis, characterization and microwave characteristics of ATP/BaFe₁₂O₁₉/PANI ternary composites. *J. Magn. Magn. Mater.* (2018). <https://doi.org/10.1016/j.jmmm.2017.12.101>
42. K. Didehban, E. Yarahmadi, F. Nouri-ahangarani, S.A. Mir-mohammadi, N. Bahri-laleh, Radar Absorption Properties of Ni_{0.5}Zn_{0.5}Fe₂O₄/PANI/epoxy. *Nanocomposites* (2015). <https://doi.org/10.1002/jccs.201500136>

Publisher's Note Springer Nature remains neutral with regard to jurisdictional claims in published maps and institutional affiliations.

Affiliations

Faezeh Tavakolinia¹ · Mohammad Yousefi² · Seyyed Salman Seyyed Afghahi³ · Saeid Baghshahi⁴ · Susan Samadi²

¹ Department of Chemistry, Science and Research Branch, Islamic Azad University, Tehran, Iran

² Department of Chemistry, Yadegar-E-Imam Khomeini (RAH) Shahre Rey Branch, Islamic Azad University, Tehran, Iran

³ Department of Engineering, Imam Hossein University, Tehran, Iran

⁴ Department of Materials Engineering, Faculty of Engineering, Imam Khomeini International University, Qazvin, Iran